Supplementary Material for "Geometric mechanics of origami patterns exhibiting Poisson's ratio switch by breaking Mountain and Valley assignment"

Phanisri P. Pratapa,[1,*] Ke Liu,[1,*] and Glaucio H. Paulino[1,†]

[1] *School of Civil and Environmental Engineering, Georgia Institute of Technology, Atlanta, GA 30332, USA*

(Dated: March 28, 2019)

* P.P.P. and K.L. contributed equally to this work.

† paulino@gatech.edu

CONTENTS

I. GEOMETRY AND CONFIGURATION SPACE OF THE MORPH PATTERN

The unit cell geometry of the Morph pattern, shown in Fig. S1(a) is characterized by the shape of the panels and the angles between them that define the folded state. The panel shapes are given by the angles α, β and edge lengths a, b, c. The nine vertices of the unit cell are numbered from O_1 to O_9.

Without loss of generality, we assume $\alpha > \beta$, which makes the $\overrightarrow{O_5O_6}$ crease to be the one that switches between mountain/valley, as indicated by the red line shown in Fig. S1(a). As shown in Figs. S1(b),(c),(d), to protect the orthorhombic nature of the unit cell, the edge lengths of adjacent panels need to be unequal (but related) except when they have the same panel angles. Hence, the edge lengths $|\overrightarrow{O_1O_4}|$ and $|\overrightarrow{O_7O_4}|$ are equal to c as they belong to panels with the same angle α. On the other hand, $|\overrightarrow{O_7O_8}|$ and $|\overrightarrow{O_9O_8}|$ cannot be equal when $\alpha \neq \beta$. As a consequence of this, the Morph pattern has only one plane of symmetry (unlike the two-fold symmetric nature of the standard eggbox).

The relation between the unequal edge lengths a, b can be obtained as follows. Consider Figs. S1(b),(c) which show the side views of the unit cell. When $h_1 (= a|\cos\phi_1|)$ and $h_2 (= b|\cos\phi_2|)$ are equal, $\overrightarrow{O_7O_9}$ is normal to the planes $(O_1O_4O_7)$ and $(O_3O_6O_9)$ which ensures that the unit cell is orthorhombic. However, this is not true when $h_1 \neq h_2$. Hence, for $h_1 = h_2$, we have,

$$\frac{a}{b} = \left|\frac{\cos\phi_2}{\cos\phi_1}\right| . \tag{S1}$$

Using spherical trigonometry of vertex O_5 (see Fig. S2(a)), we have,

$$\cos\alpha = \cos\frac{\psi}{2}\cos\phi_1 , \tag{S2}$$

$$\cos\beta = \cos\frac{\psi}{2}\cos\phi_2 . \tag{S3}$$

This is true due to the plane of symmetry that bisects the dihedral angles γ_1, γ_3 and therefore angle ψ. Combining the above two equations, we get,

$$\frac{\cos\phi_2}{\cos\phi_1} = \frac{\cos\beta}{\cos\alpha} . \tag{S4}$$

Finally, from Eqns. S1 and S4, we get,

$$\frac{a}{b} = \left|\frac{\cos\beta}{\cos\alpha}\right| . \tag{S5}$$

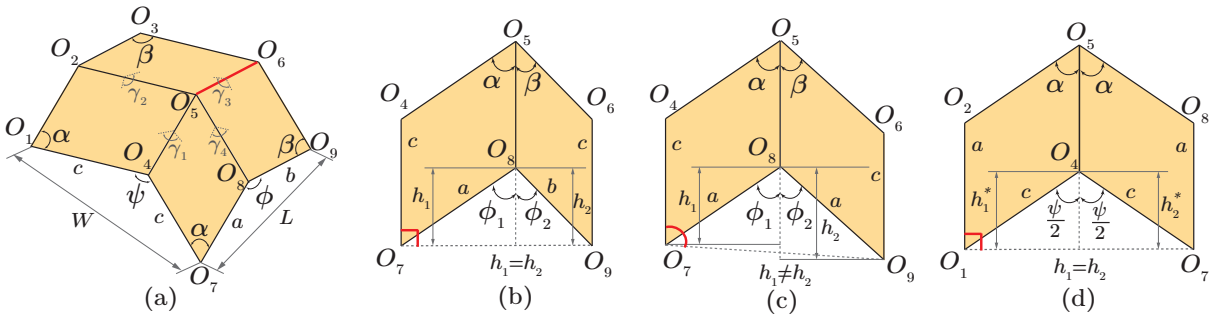

FIG. S1. (a) Geometry of the Morph unit cell. (b), (c), (d) Side views of the unit cell. (b) $\overrightarrow{O_7O_9}$ is normal to the plane $(O_1O_4O_7)$ as $h_1 = h_2$, i.e., $a\cos\phi_1 = b\cos\phi_2$. (c) $\overrightarrow{O_7O_9}$ is not normal to the plane $(O_1O_4O_7)$ as $h_1 \neq h_2$ (since $\phi_1 \neq \phi_2$ for $\alpha \neq \beta$). We avoid this case to maintain the orthorhombic nature of the unit cell by making $|\overrightarrow{O_7O_8}| \neq |\overrightarrow{O_9O_8}|$. (d) $\overrightarrow{O_1O_7}$ is normal to the plane $(O_1O_2O_3)$ as $h_1^* = h_2^* = c\cos(\psi/2)$.

Therefore, in order to ensure that the triangular faces $(O_1O_2O_3)$, $(O_3O_6O_9)$, $(O_1O_4O_7)$, $(O_7O_8O_9)$ are all orthogonal to the base of the unit cell $(O_1O_7O_9O_3)$, we only consider geometries with $b|\cos\beta| = a|\cos\alpha|$ so that,

$$b = a\left|\frac{\cos\alpha}{\cos\beta}\right| . \tag{S6}$$

The length L and width W of the unit cell are given by,

$$W = 2c\sin\frac{\psi}{2} , \tag{S7}$$

$$L = \sqrt{a^2 + b^2 - 2ab\cos\phi} , \tag{S8}$$

where, ϕ, ψ are the angles between the opposite crease lines. The folded state of the system is given by any of ϕ, ψ or the dihedral angles γ_1, γ_2, γ_3, γ_4 all of which can be related to one another through the following equations obtained using the spherical law of cosines at vertex O_5 (see Fig. S2(b)):

$$\cos\psi = \cos^2\alpha + \sin^2\alpha\cos\gamma_1 , \tag{S9}$$

$$\cos\psi = \cos^2\beta + \sin^2\beta\cos\gamma_3 , \tag{S10}$$

$$\cos\phi = \cos\alpha\cos\beta + \sin\alpha\sin\beta\cos\gamma_2 , \tag{S11}$$

$$\cos\phi = \cos\alpha\cos\beta + \sin\alpha\sin\beta\cos\gamma_4 . \tag{S12}$$

The configuration space that describes the morphing between eggbox and Miura modes is understood in terms of the relation between ϕ and ψ, which can be derived as follows.

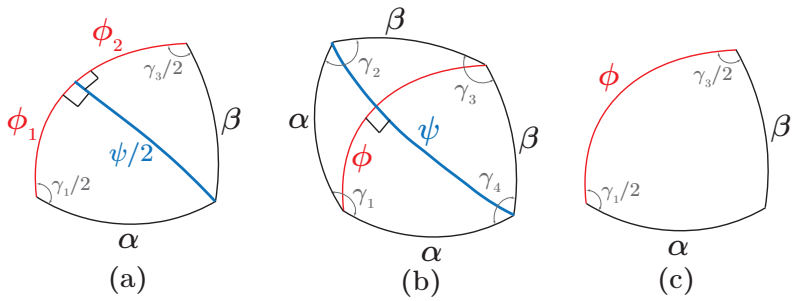

FIG. S2. The spherical trigonometric representation of the vertex O_5 formed by the: (a) Intersection of planes $(O_4O_5O_6)$, $(O_4O_5O_8)$ and $(O_8O_5O_6)$. The plane $(O_2O_5O_8) \parallel (O_1O_4O_7)$ in which ψ is measured is orthogonal to the plane $(O_4O_5O_6)$ in which ϕ_1 and ϕ_2 are measured. (b) Intersection of planes $(O_4O_5O_8)$, $(O_4O_5O_2)$, $(O_2O_5O_6)$ and $(O_8O_5O_6)$. The planes $(O_4O_5O_6)$ and $(O_2O_5O_8)$ in which ϕ and ψ are respectively measured are orthogonal to each other. (c) Intersection of planes $(O_4O_5O_6)$, $(O_4O_5O_8)$ and $(O_8O_5O_6)$.

From Eqns. S11 and S12, we have $\gamma_2 = \gamma_4$ indicating the presence of a plane of symmetry $(O_4O_5O_6)$ which bisects the dihedral angles γ_1 and γ_3. Using spherical trigonometry at vertex O_5 (see Fig. S2(c)), the spherical law of cosines gives,

$$\cos\beta = \cos\alpha\cos\phi + \sin\alpha\sin\phi\cos\left(\frac{\gamma_1}{2}\right), \tag{S13}$$

$$\cos\alpha = \cos\beta\cos\phi + \sin\beta\sin\phi\cos\left(\frac{\gamma_3}{2}\right). \tag{S14}$$

Let us define two intermediate variables:

$$\xi = \cos\beta - \cos\alpha\cos\phi = \sin\alpha\sin\phi\cos(\gamma_1/2), \tag{S15}$$

$$\zeta = \cos\alpha - \cos\beta\cos\phi = \sin\beta\sin\phi\cos(\gamma_3/2). \tag{S16}$$

This gives us,

$$\cos\gamma_1 = \left(\frac{2\xi^2}{\sin^2\alpha\sin^2\phi} - 1\right). \tag{S17}$$

Combing the above equation with Eqn. S9, we get,

$$\cos\psi = \cos 2\alpha + \frac{2\xi^2}{\sin^2\phi}. \tag{S18}$$

Therefore, we can also derive,

$$\frac{\mathrm{d}\psi}{\mathrm{d}\phi} = -\frac{4(\cos\beta - \cos\alpha\cos\phi)(\cos\alpha - \cos\beta\cos\phi)}{\sin\psi\sin^3\phi} = -\frac{4\xi\zeta}{\sin\psi\sin^3\phi}. \tag{S19}$$

From Eqn. S15, $\xi > 0$ since, $\gamma_1 < \pi$ throughout the configurational space. Hence, the sign of the above derivative depends only on the sign of ζ. For $\gamma_3 > \pi$ (Miura mode), $\zeta < 0$, making $\mathrm{d}\psi/\mathrm{d}\phi > 0$. This derivative is used in the derivation of the Poisson's ratio in stretch, ν^s_{WL}, which is defined as:

$$\nu^s_{WL} = -\frac{\epsilon_W}{\epsilon_L} = -\frac{\mathrm{d}W/W}{\mathrm{d}L/L} = -\frac{L}{W}\frac{\mathrm{d}W}{\mathrm{d}L} = -\frac{L}{W}\left(\frac{\mathrm{d}W/\mathrm{d}\psi}{\mathrm{d}L/\mathrm{d}\phi}\right)\frac{\mathrm{d}\psi}{\mathrm{d}\phi} = \frac{4c^2L^2}{a^2W^2}\left|\frac{\cos\beta}{\cos\alpha}\right|\frac{\xi\zeta}{\sin^4\phi}\,. \quad \text{(S20)}$$

The experimental verification of the Poisson's ratio is demonstrated indirectly by measuring the unit cell dimensions as shown in Fig. S3.

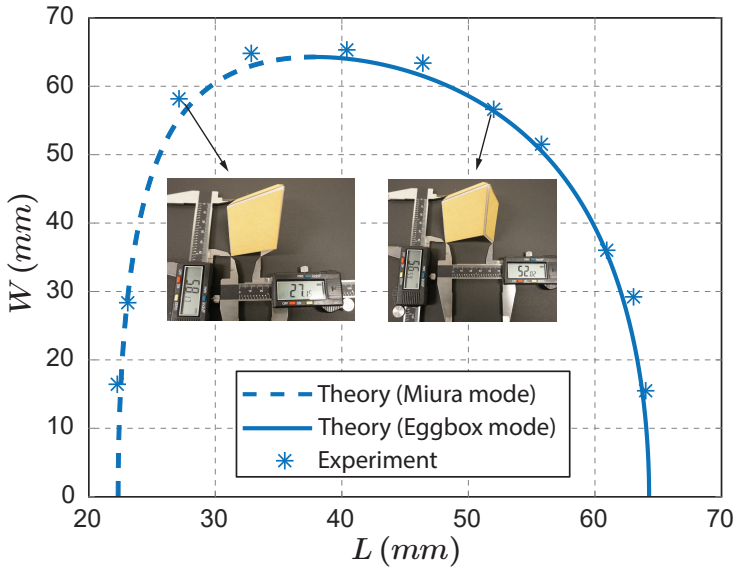

FIG. S3. Comparison between the theoretical description and experimental measurements of the Morph unit cell geometry. The slope of the L vs. W curve describes the Poisson effects since, $\nu^s_{WL} = -(L/W)(\mathrm{d}W/\mathrm{d}L)$. The slope in the Miura mode is positive and that in the eggbox mode is negative which leads to the Poisson's ratios that are negative and positive respectively. The panel dimensions were chosen to be $a = c = 5\,mm$ with panel angles $\alpha = 60°$ and $\beta = 40°$ for the prototype.

II. IN-PLANE STIFFNESS OF THE MORPH PATTERN

Folding of the Morph results in planar kinematics that keeps the global configuration of an assemblage staying flat. If we assign elasticity to the folding hinges, we can obtained the in-plane stiffness of the assemblage. We look at the stiffness of a single unit cell here

(essentially one vertex with 4 folding hinges). Let the energy per unit length in the rotational hinges be given by $\mathcal{E}(\gamma_i) = \frac{1}{2}k_f(\gamma_i - \gamma_{i,0})^2$ for $i = 1, 2, 3, 4$, where, $\gamma_{i,0}$ denotes the neutral angles in the undeformed configuration and k_f is the folding stiffness constant per unit length associated with the rotational hinges. Due to symmetry, $\gamma_2 = \gamma_4$, and we have the total energy of the unit cell in stretch given by,

$$\begin{aligned}\mathcal{U}_s &= a\mathcal{E}(\gamma_1) + b\mathcal{E}(\gamma_3) + 2c\mathcal{E}(\gamma_2) \\ &= \frac{k_f}{2}\left[a(\gamma_1 - \gamma_{1,0})^2 + b(\gamma_3 - \gamma_{3,0})^2 + 2c(\gamma_2 - \gamma_{2,0})^2\right] .\end{aligned} \tag{S21}$$

As the in-plane deformation of the unit cell can be described using a single degree of freedom, γ_3 and γ_2 can be expressed in terms of γ_1 and we can evaluate the derivatives of the energy as:

$$\frac{\mathrm{d}^2\mathcal{U}_s}{\mathrm{d}W^2} = \frac{\mathrm{d}^2\mathcal{U}_s}{\mathrm{d}\gamma_1^2}\left(\frac{\mathrm{d}W}{\mathrm{d}\gamma_1}\right)^{-2} - \frac{\mathrm{d}\mathcal{U}_s}{\mathrm{d}\gamma_1}\frac{\mathrm{d}^2W}{\mathrm{d}\gamma_1^2}\left(\frac{\mathrm{d}W}{\mathrm{d}\gamma_1}\right)^{-3}, \tag{S22}$$

$$\frac{\mathrm{d}^2\mathcal{U}_s}{\mathrm{d}L^2} = \frac{\mathrm{d}^2\mathcal{U}_s}{\mathrm{d}\gamma_1^2}\left(\frac{\mathrm{d}L}{\mathrm{d}\gamma_1}\right)^{-2} - \frac{\mathrm{d}\mathcal{U}_s}{\mathrm{d}\gamma_1}\frac{\mathrm{d}^2L}{\mathrm{d}\gamma_1^2}\left(\frac{\mathrm{d}L}{\mathrm{d}\gamma_1}\right)^{-3}. \tag{S23}$$

We can derive that,

$$\frac{\mathrm{d}\mathcal{U}_s}{\mathrm{d}\gamma_1} = a\mathcal{E}'(\gamma_1) + b\mathcal{E}'(\gamma_3)\left(\frac{\mathrm{d}\gamma_3}{\mathrm{d}\gamma_1}\right) + 2c\mathcal{E}'(\gamma_2)\left(\frac{\mathrm{d}\gamma_2}{\mathrm{d}\gamma_1}\right), \tag{S24}$$

$$\frac{\mathrm{d}^2\mathcal{U}_s}{\mathrm{d}\gamma_1^2} = a\mathcal{E}''(\gamma_1) + b\mathcal{E}''(\gamma_3)\left(\frac{\mathrm{d}\gamma_3}{\mathrm{d}\gamma_1}\right)^2 + 2c\mathcal{E}''(\gamma_2)\left(\frac{\mathrm{d}\gamma_2}{\mathrm{d}\gamma_1}\right)^2 + b\mathcal{E}'(\gamma_3)\left(\frac{\mathrm{d}^2\gamma_3}{\mathrm{d}\gamma_1^2}\right) + 2c\mathcal{E}'(\gamma_2)\left(\frac{\mathrm{d}^2\gamma_2}{\mathrm{d}\gamma_1^2}\right), \tag{S25}$$

where, $\mathcal{E}'(\gamma_i) = k_f(\gamma_i - \gamma_{i,0})$ and $\mathcal{E}''(\gamma_i) = k_f$. Noting that, $\frac{\mathrm{d}\mathcal{U}_s}{\mathrm{d}\gamma_1}\big|_{\gamma_1=\gamma_{1,0}} = 0$, we define the stiffness along **W** and **L** directions as follows:

$$K_W = \left.\frac{\mathrm{d}^2\mathcal{U}_s}{\mathrm{d}W^2}\right|_{\gamma_1=\gamma_{1,0}} = \left.\frac{\mathrm{d}^2\mathcal{U}_s}{\mathrm{d}\gamma_1^2}\right|_{\gamma_1=\gamma_{1,0}}\left(\left.\frac{\mathrm{d}W}{\mathrm{d}\gamma_1}\right|_{\gamma_1=\gamma_{1,0}}\right)^{-2}, \tag{S26}$$

$$K_L = \left.\frac{\mathrm{d}^2\mathcal{U}_s}{\mathrm{d}L^2}\right|_{\gamma_1=\gamma_{1,0}} = \left.\frac{\mathrm{d}^2\mathcal{U}_s}{\mathrm{d}\gamma_1^2}\right|_{\gamma_1=\gamma_{1,0}}\left(\left.\frac{\mathrm{d}L}{\mathrm{d}\gamma_1}\right|_{\gamma_1=\gamma_{1,0}}\right)^{-2}. \tag{S27}$$

We have,

$$\left.\frac{\mathrm{d}^2\mathcal{U}_s}{\mathrm{d}\gamma_1^2}\right|_{\gamma_1=\gamma_{1,0}} = ak_f + bk_f\left(\left.\frac{\mathrm{d}\gamma_3}{\mathrm{d}\gamma_1}\right|_{\gamma_1=\gamma_{1,0}}\right)^2 + 2ck_f\left(\left.\frac{\mathrm{d}\gamma_2}{\mathrm{d}\gamma_1}\right|_{\gamma_1=\gamma_{1,0}}\right)^2. \tag{S28}$$

One can derive,

$$\left.\frac{\mathrm{d}\gamma_3}{\mathrm{d}\gamma_1}\right|_{\gamma_1=\gamma_{1,0}} = \frac{\cos\beta - \cos\alpha\cos\phi_0}{\cos\alpha - \cos\beta\cos\phi_0}, \tag{S29}$$

$$\left.\frac{\mathrm{d}\gamma_2}{\mathrm{d}\gamma_1}\right|_{\gamma_1=\gamma_{1,0}} = \frac{-\sin^2\phi_0}{2(\cos\alpha - \cos\beta\cos\phi_0)}, \tag{S30}$$

$$\left.\frac{\mathrm{d}W}{\mathrm{d}\gamma_1}\right|_{\gamma_1=\gamma_{1,0}} = \frac{c(\cos\beta - \cos\alpha\cos\phi_0)}{\sin\phi_0}, \tag{S31}$$

$$\left.\frac{\mathrm{d}L}{\mathrm{d}\gamma_1}\right|_{\gamma_1=\gamma_{1,0}} = \frac{-ab\sin\alpha\sin\beta\sin\gamma_{2,0}\sin^2\phi_0}{2L_0(\cos\alpha - \cos\beta\cos\phi_0)}, \tag{S32}$$

where ϕ_0, L_0 correspond to ϕ and L respectively when $\gamma_i = \gamma_{i,0}$. By combining Eqn. S28 with Eqns. S26 and S27, we have,

$$K_W = ak_f\left(\left.\frac{\mathrm{d}\gamma_1}{\mathrm{d}W}\right|_{\gamma_1=\gamma_{1,0}}\right)^2 + bk_f\left(\left.\frac{\mathrm{d}\gamma_3}{\mathrm{d}W}\right|_{\gamma_1=\gamma_{1,0}}\right)^2 + 2ck_f\left(\left.\frac{\mathrm{d}\gamma_2}{\mathrm{d}W}\right|_{\gamma_1=\gamma_{1,0}}\right)^2, \tag{S33}$$

$$K_L = ak_f\left(\left.\frac{\mathrm{d}\gamma_1}{\mathrm{d}L}\right|_{\gamma_1=\gamma_{1,0}}\right)^2 + bk_f\left(\left.\frac{\mathrm{d}\gamma_3}{\mathrm{d}L}\right|_{\gamma_1=\gamma_{1,0}}\right)^2 + 2ck_f\left(\left.\frac{\mathrm{d}\gamma_2}{\mathrm{d}L}\right|_{\gamma_1=\gamma_{1,0}}\right)^2. \tag{S34}$$

The normalized stiffnesses are obtained as K_W/k_f and K_L/k_f.

Below, we present the analytical expressions for the in-plane stiffnesses of standard eggbox and Miura-ori, obtained as particular cases from the above results.

A. Reduction to standard eggbox

For standard eggbox, by using, $a = b = c$ and $\beta = \alpha$ in Eqns. S33, S34, we get:

$$K_W = \frac{2k_f}{a}\left(\frac{\cos^2(\phi/2) + \cos^2(\psi/2)}{\sin^2(\phi/2)\cos^4(\psi/2)}\right), \tag{S35}$$

$$K_L = \frac{2k_f}{a}\left(\frac{\cos^2(\phi/2) + \cos^2(\psi/2)}{\sin^2(\psi/2)\cos^4(\phi/2)}\right). \tag{S36}$$

B. Reduction to standard Miura-ori

For standard Miura-ori, by using, $a = b = c$ and $\beta = \pi - \alpha$ in Eqns. S33, S34, we get:

$$K_W = \frac{2k_f}{a}\left(\frac{\sin^2(\phi/2) + \cos^2(\psi/2)}{\cos^2(\phi/2)\cos^4(\psi/2)}\right), \tag{S37}$$

$$K_L = \frac{2k_f}{a}\left(\frac{\sin^2(\phi/2) + \cos^2(\psi/2)}{\cos^2(\phi/2)\sin^2(\psi/2)\sin^2(\phi/2)}\right). \tag{S38}$$

III. OUT-OF-PLANE BENDING OF STANDARD EGGBOX

Before we discuss the out-of-plane bending of the Morph pattern, we derive bending Poisson's ratio of the standard eggbox tessellation and show that it depends only on the bending of the panels. This observation allows for a simplified treatment of bending in the generalized case leading to the Morph pattern. The following derivation is inspired from the bending curvature calculations for Miura-ori tessellation [1]. In this context, bending of the origami unit cell is enabled by applying infinitesimal rotations about the fold lines and diagonals of the panels.

A. Coordinate system and infinitesimal rotations

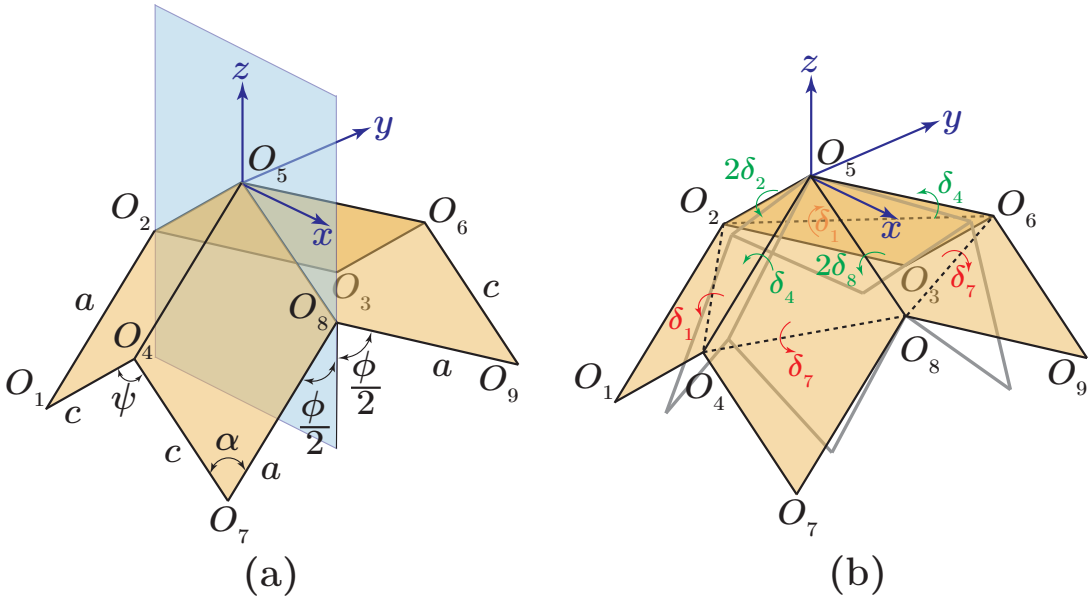

FIG. S4. Standard eggbox unit cell. (a) Undeformed configuration and the xz-plane of symmetry of the unit cell. (b) Infinitesimal rotations and the deformed configuration (wire-frame) under bending. The rotations about the panel diagonals (dashed lines) are shown in red and those about the fold lines are shown in green.

The schematic of a standard eggbox unit cell with and without infinitesimal rotations is shown in Fig. S4. The geometry of the undeformed unit cell is dictated by the panel angle α, the edge lengths a, c, and any of the folding angles ϕ or ψ. We assume a coordinate

system with origin at O_5 as shown in the figure. We fix the vertices O_5 and O_8 to avoid any rigid body motions while applying bending deformations. Further, we note that there exists a plane of symmetry formed by the vectors $\overrightarrow{O_5O_8}$ and $\overrightarrow{O_5O_2}$. The coordinates of the fixed vertices O_5 and O_8 are:

$$
\begin{aligned}
(O_{5x}, O_{5y}, O_{5z}) &= (0, 0, 0)\,, \\
(O_{8x}, O_{8y}, O_{8z}) &= (c\sin\frac{\psi}{2}, 0, -c\cos\frac{\psi}{2})\,.
\end{aligned}
$$

The coordinates of the other vertices in the undeformed configuration are:

$$
\begin{aligned}
(O_{7x}, O_{7y}, O_{7z}) &= (c\sin\frac{\psi}{2}, -a\sin\frac{\phi}{2}, -c\cos\frac{\psi}{2} - a\cos\frac{\phi}{2})\,, \\
(O_{4x}, O_{4y}, O_{4z}) &= (0, -a\sin\frac{\phi}{2}, -a\cos\frac{\phi}{2})\,, \\
(O_{1x}, O_{1y}, O_{1z}) &= (-c\sin\frac{\psi}{2}, -a\sin\frac{\phi}{2}, -c\cos\frac{\psi}{2} - a\cos\frac{\phi}{2})\,, \\
(O_{2x}, O_{2y}, O_{2z}) &= (-c\sin\frac{\psi}{2}, 0, -c\cos\frac{\psi}{2})\,,
\end{aligned}
$$

The coordinates of the remaining vertices O_3, O_6, O_9 can be obtained through symmetry.

In order to find out the coordinates of the vertices after the infinitesimal rotations are applied, we use the Rodrigues' rotational formula for small rotations [1]:

$$
\begin{aligned}
x' &= x + [m(z-w) - n(y-v)]\,\delta\,, \\
y' &= y - [l(z-w) - n(x-u)]\,\delta\,, \\
z' &= z + [l(y-v) - m(x-u)]\,\delta\,,
\end{aligned}
\tag{S39}
$$

where, (x', y', z') are the coordinates of a point (x, y, z) after an infinitesimal rotation of δ ($\delta \ll 1$) about an axis with direction cosines $[l, m, n]$ and passing through a point (u, v, w).

It is sufficient to calculate the effect of rotations δ_8, δ_7, δ_4 and δ_1 on one side of the symmetry plane. Additionally, δ_2 is compatible with the rest of the rotations, i.e. the rotations δ_8, δ_7, δ_4 and δ_1 will result in an effective rotation of δ_2 about $\overrightarrow{O_2O_5}$ on one side of the symmetry plane. Using the above Rodrigues' formula, the coordinates of the vertices after applying the bending inducing rotations are obtained as:

$$
\begin{aligned}
O'_{4x} &= -(a\sin\frac{\phi}{2}\cos\frac{\psi}{2})\delta_8\,, \\
O'_{4y} &= -a\sin\frac{\phi}{2} + (a\sin\frac{\psi}{2}\cos\frac{\phi}{2})\delta_8\,, \\
O'_{4z} &= -a\cos\frac{\phi}{2} - (a\sin\frac{\phi}{2}\sin\frac{\psi}{2})\delta_8\,,
\end{aligned}
\tag{S40}
$$

$$
\begin{aligned}
O'_{2x} &= -c\sin\frac{\psi}{2} + (c\sin\frac{\phi}{2}\cos\frac{\psi}{2})\delta_4\,,\\
O'_{2y} &= (2c\sin\frac{\psi}{2}\cos\frac{\psi}{2})\delta_8 + (c\sin\frac{\psi}{2}\cos\frac{\phi}{2})\delta_4\,,\\
O'_{2z} &= -a\cos\frac{\psi}{2} - (c\sin\frac{\psi}{2}\sin\frac{\phi}{2})\delta_4\,,
\end{aligned}
\tag{S41}
$$

$$
\begin{aligned}
O'_{7x} &= c\sin\frac{\psi}{2} - (a\sin\frac{\phi}{2}\cos\frac{\psi}{2})\delta_8 - (ac\sin\frac{\phi}{2}\cos\frac{\psi}{2})(\delta_7/\ell)\,,\\
O'_{7y} &= -a\sin\frac{\phi}{2} + (a\sin\frac{\psi}{2}\cos\frac{\phi}{2})\delta_8 + (ac\sin\frac{\psi}{2}\cos\frac{\phi}{2})(\delta_7/\ell)\,,\\
O'_{7z} &= -(a\cos\frac{\phi}{2} + c\cos\frac{\psi}{2}) - (a\sin\frac{\phi}{2}\sin\frac{\psi}{2})\delta_8 - (ac\sin\frac{\phi}{2}\sin\frac{\psi}{2})(\delta_7/\ell)\,,
\end{aligned}
\tag{S42}
$$

$$
\begin{aligned}
O'_{1x} &= -c\sin\frac{\psi}{2} - (a\sin\frac{\phi}{2}\cos\frac{\psi}{2})\delta_8 + (c\sin\frac{\phi}{2}\cos\frac{\psi}{2})\delta_4 + (ac\sin\frac{\phi}{2}\cos\frac{\psi}{2})(\delta_1/\ell)\,,\\
O'_{1y} &= -a\sin\frac{\phi}{2} + (a\sin\frac{\psi}{2}\cos\frac{\phi}{2} + 2c\sin\frac{\psi}{2}\cos\frac{\psi}{2})\delta_8 + (c\sin\frac{\psi}{2}\cos\frac{\phi}{2})\delta_4 + (ac\sin\frac{\psi}{2}\cos\frac{\phi}{2})(\delta_1/\ell)\,,\\
O'_{1z} &= -(a\cos\frac{\phi}{2} + c\cos\frac{\psi}{2}) - (a\sin\frac{\phi}{2}\sin\frac{\psi}{2})\delta_8 - (c\sin\frac{\psi}{2}\sin\frac{\phi}{2})\delta_4 - (ac\sin\frac{\phi}{2}\sin\frac{\psi}{2})(\delta_1/\ell)\,,
\end{aligned}
\tag{S43}
$$

where, $\ell = \sqrt{a^2 + c^2 - 2ac\cos\alpha}$ is the length of the panel's shorter diagonal.

Using symmetry in the standard eggbox unit cell, we have the following two conditions:

$$
O'_{2y} = 0 \implies \delta_4 = -\frac{2\cos(\psi/2)}{\cos(\phi/2)}\delta_8\,, \tag{S44}
$$

$$
O'_{7y} = O'_{1y} \implies \delta_7 = \delta_1\,. \tag{S45}
$$

B. Curvatures and Poisson's ratio in bending

The curvature in the x or y direction is defined by the change in the dihedral angle between the opposing triangular faces divided by the length of the unit cell. The curvature in the x direction is calculated as,

$$
\begin{aligned}
\kappa_x = \frac{\Delta\text{Dihedral}}{\Delta x} &= -\frac{1}{W}\left[\left(\frac{O_{8x} - \left(\frac{O'_{9x}+O'_{7x}}{2}\right)}{O_{8z} - \left(\frac{O'_{9z}+O'_{7z}}{2}\right)}\right) - \left(\frac{O'_{2x} - \left(\frac{O'_{3x}+O'_{1x}}{2}\right)}{O'_{2z} - \left(\frac{O'_{3z}+O'_{1z}}{2}\right)}\right)\right]\\
&= -\frac{1}{2c\sin(\psi/2)}\left[\left(\frac{O_{8x} - O'_{7x}}{O_{8z} - O'_{7z}}\right) - \left(\frac{O'_{2x} - O'_{1x}}{O'_{2z} - O'_{1z}}\right)\right].
\end{aligned}
\tag{S46}
$$

The curvature in the y direction is calculated as,

$$\kappa_y = \frac{\Delta\text{Dihedral}}{\Delta y} = -\frac{1}{L}\left[\left(\frac{O'_{6y} - \left(\frac{O'_{3y}+O'_{9y}}{2}\right)}{O'_{6z} - \left(\frac{O'_{3z}+O'_{9z}}{2}\right)}\right) - \left(\frac{O'_{4y} - \left(\frac{O'_{7y}+O'_{1y}}{2}\right)}{O'_{4z} - \left(\frac{O'_{7z}+O'_{1z}}{2}\right)}\right)\right]$$
$$= -\frac{1}{2a\sin(\phi/2)}\left[\left(-2\left(\frac{O'_{4y} - O'_{7y}}{O'_{4z} - O'_{7z}}\right)\right)\right]. \tag{S47}$$

Using Eqns. S44 and S45 and evaluating the above expressions, we get,

$$\kappa_x = -\frac{\tan(\phi/2)}{\tan(\psi/2)}\frac{\delta_1}{\ell}, \tag{S48}$$

$$\kappa_y = -\frac{\tan(\psi/2)}{\tan(\phi/2)}\frac{\delta_1}{\ell}. \tag{S49}$$

The Poisson's ratio of the standard eggbox cell in bending (defined as the ratio of curvatures [1, 2]) can be obtained as,

$$\nu^b_{WL} = -\frac{\kappa_x}{\kappa_y} = -\frac{\tan^2(\phi/2)}{\tan^2(\psi/2)}. \tag{S50}$$

This result is in agreement with that obtained by [3]. *We note that the curvatures are independent of the infinitesimal rotations δ_4, δ_8 across the fold lines.* They only depend on δ_1 (or δ_7) about the panel diagonals. Also, from Eqns. S44 and S45, δ_1 and δ_7 are independent of δ_4 and δ_8. This indicates that it is sufficient to consider infinitesimal rotations causing panel bending to calculate curvatures and bending Poisson's ratio of eggbox type cells. A similar observation also applies to standard Miura-ori pattern.

In reference [1], infinitesimal rotations are applied about the fold lines and diagonals of the panels. However, from the aforementioned discussion, it is sufficient to consider only infinitesimal rotations along the panel diagonals. This is the approach followed in the remainder of this paper.

IV. OUT-OF-PLANE BENDING OF THE MORPH PATTERN

The procedure described above for standard eggbox is too specific and cannot be readily applied to systems which do not share so many symmetries as standard eggbox or Miura-ori. Hence, in this section, we develop a general approach for representing the coordinates of the vertices and calculation of curvatures and apply the concept to the case of the Morph unit cell.

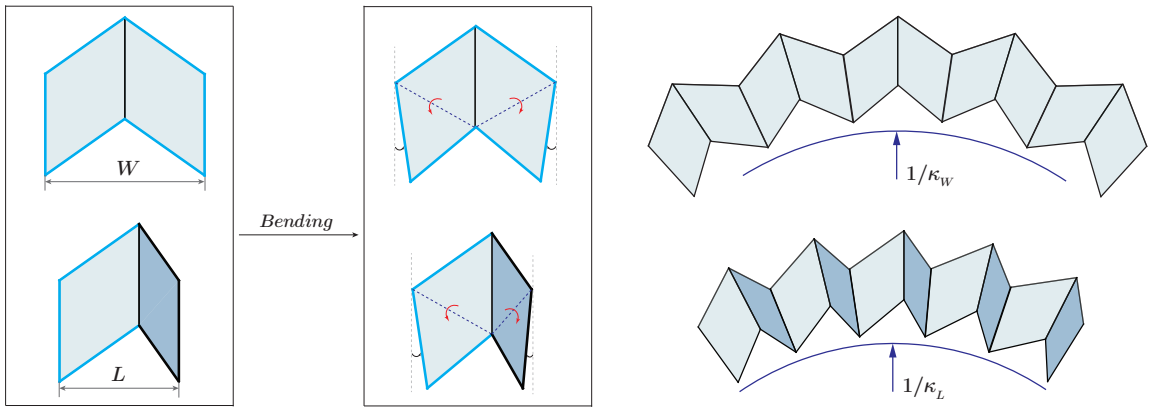

FIG. S5. Bending of Morph in eggbox mode. Curvatures along both **W** and **L** directions are of the same sign.

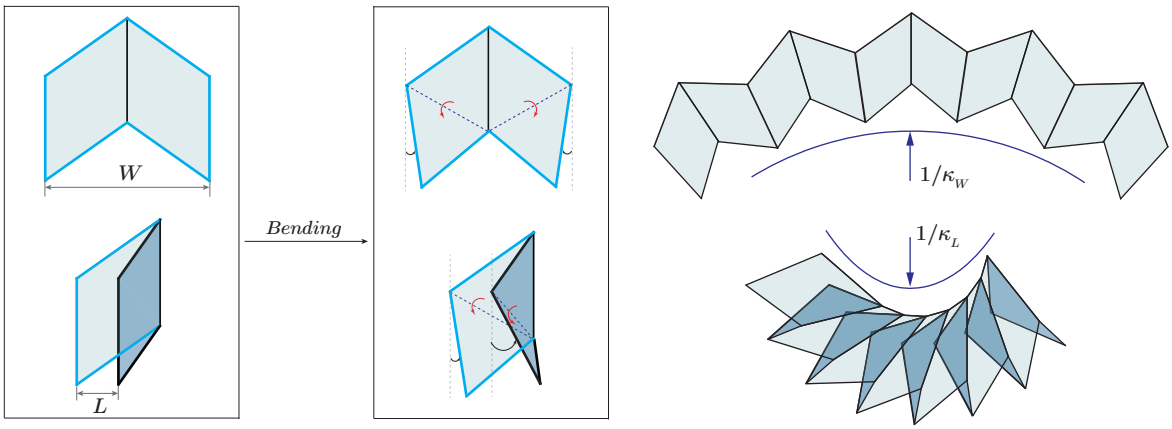

FIG. S6. Bending of Morph in Miura mode. Curvatures along **W** and **L** directions are of opposite sign.

The schematic of the curvatures induced along the **W** and **L** directions due to bending of the Morph pattern are shown in Figs. S5 and S6. As shown in the previous section, it is sufficient to consider infinitesimal rotations along the diagonals of the panels to describe the bending of eggbox cell. Hence, for the Morph unit cell, we fix the positions of vertices O_2, O_4, O_5, O_6, and O_8 while applying panel bending through rotations δ_1, δ_2, δ_3 and δ_4 across diagonals $\overrightarrow{O_2O_4}$, $\overrightarrow{O_6O_2}$, $\overrightarrow{O_8O_6}$, and $\overrightarrow{O_4O_8}$ respectively, (see Fig. S7(a)). Accordingly, the vertices O_1, O_3, O_9 and O_7 are displaced to O_1', O_3', O_9' and O_7' respectively.

A. Coordinate system, vertices and normals

As shown in Fig. S7(b), we assume a coordinate system with origin at vertex O_5 and x-axis along the fold line $\overrightarrow{O_2O_5}$. The xy-plane is assumed to coincide with panel $(O_1O_2O_5O_4)$ and z-axis is obtained by the right hand rule. The coordinates of all the vertices in this system can be obtained in terms of the panel edge lengths (a, b, c), the panel angles (α, β) and the dihedral angles (γ_i, $i = 1, 2, 3, 4$) using the Rodrigues' rotation formula for finite rotations [4]:

$$\overrightarrow{\mathbf{v}}_{rot} = \overrightarrow{\mathbf{v}}\cos\eta + (\hat{\mathbf{p}} \times \overrightarrow{\mathbf{v}})\sin\eta + \hat{\mathbf{p}}(\hat{\mathbf{p}} \cdot \overrightarrow{\mathbf{v}})(1 - \cos\eta)\,, \tag{S51}$$

where, $\overrightarrow{\mathbf{v}}_{rot}$ is obtained by rotating a vector $\overrightarrow{\mathbf{v}}$ about axis of rotation $\hat{\mathbf{p}}$ by an angle η using the right hand rule. We note that the above formula reduces to Eqn. S39 for small rotations when $\eta = \delta \to 0$. Using this formula, the coordinates of vertices on the triangular face $(O_1O_2O_3)$ are obtained as:

$$\begin{aligned}
O_2 &= (-c, 0, 0)\,,\\
O_1 &= (-c - a\cos\alpha, -a\sin\alpha, 0)\,,\\
O_3 &= (-c - b\cos\beta, -b\cos\gamma_2\sin\beta, -b\sin\gamma_2\sin\beta)\,.
\end{aligned}$$

The coordinates of O_1 and O_3 after applying the infinitesimal rotations δ_1 (about $\overrightarrow{O_2O_4}$) and δ_2 (about $\overrightarrow{O_6O_2}$) are obtained using Eqn. S39 as,

$$\begin{aligned}
O_1' &= (-c - a\cos\alpha, -a\sin\alpha, -(ac\sin\alpha)\frac{\delta_1}{\ell_1})\,,\\
O_3' &= (-c - b\cos\beta, -b\cos\gamma_2\sin\beta - (cb\sin\gamma_2\sin\beta)\frac{\delta_2}{\ell_2}, -b\sin\gamma_2\sin\beta + (cb\cos\gamma_2\sin\beta)\frac{\delta_2}{\ell_2})\,.
\end{aligned}$$

The normals of the triangular face $(O_1O_2O_3)$ before and after bending are calculated as

$$\begin{aligned}
\mathbf{N}_{123} &= \overrightarrow{O_2O_3} \times \overrightarrow{O_2O_1}\\
&= -ab\Big[\sin\alpha\sin\gamma_2\sin\beta\Big]\hat{\mathbf{i}} + ab\Big[\cos\alpha\sin\gamma_2\sin\beta\Big]\hat{\mathbf{j}} - ab\Big[\cos\alpha\cos\gamma_2\sin\beta - \sin\alpha\cos\beta\Big]\hat{\mathbf{k}}\,,\\
\mathbf{N}'_{123} &= \overrightarrow{O_2O_3'} \times \overrightarrow{O_2O_1'}\\
&= -ab\Big[\sin\alpha\sin\gamma_2\sin\beta - (c\sin\alpha\cos\gamma_2\sin\beta)(\frac{\delta_2}{\ell_2} + \frac{\delta_1}{\ell_1})\Big]\hat{\mathbf{i}}\\
&\quad + ab\Big[\cos\alpha\sin\gamma_2\sin\beta - (c\cos\alpha\cos\gamma_2\sin\beta)\frac{\delta_2}{\ell_2} - (c\sin\alpha\cos\beta)\frac{\delta_1}{\ell_1}\Big]\hat{\mathbf{j}}\\
&\quad - ab\Big[\cos\alpha\cos\gamma_2\sin\beta - \sin\alpha\cos\beta + (c\cos\alpha\sin\gamma_2\sin\beta)\frac{\delta_2}{\ell_2}\Big]\hat{\mathbf{k}}\,,
\end{aligned}$$

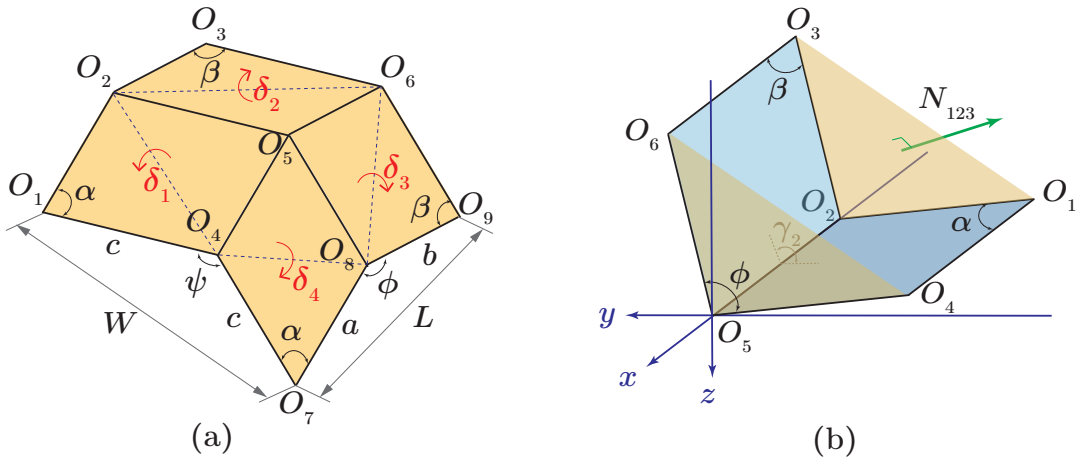

FIG. S7. (a) Infinitesimal rotations about panel diagonals to model bending. (b) Local coordinate system used to calculate the normals and the angle change for the triangular face ($O_1O_2O_3$).

where, $\hat{\mathbf{i}}$, $\hat{\mathbf{j}}$, $\hat{\mathbf{k}}$ are the unit vectors along the x, y, z axes.

B. Constraints on bending rotations

The bending of the tessellation preserves the orthogonality of the unit cell (i.e. $\mathbf{L} \cdot \mathbf{W} = 0$). Hence, we enforce the constraint that the normals of the triangular faces ($O_1O_2O_3$), ($O_3O_6O_9$), ($O_1O_4O_7$), ($O_7O_8O_9$) before and after panel bending are orthogonal to their respective base edges. We impose,

$$(\mathbf{N}'_{123} - \mathbf{N}_{123}) \cdot \overrightarrow{O_1O_3} = \Delta\mathbf{N}_{123} \cdot \overrightarrow{O_1O_3} = 0\,, \tag{S52}$$

since, $\mathbf{N}_{123} \perp \overrightarrow{O_1O_3}$. After evaluating the above constraint, we arrive at a relation between the panel bending rotations δ_1 and δ_2 (since, $\mathbf{N}'_{123}$ only depends on the rotations δ_1, δ_2.):

$$\frac{\delta_2}{\ell_2} b\zeta = \frac{\delta_1}{\ell_1} a\xi\,. \tag{S53}$$

Using the above mentioned procedure for the other triangular faces and the relation between a and b (Eqn. S6), we have the following constraints on the bending rotations:

$$\frac{\delta_2}{\ell_2}|\cos\alpha|\zeta = \frac{\delta_1}{\ell_1}|\cos\beta|\xi\,, \tag{S54}$$

$$\frac{\delta_4}{\ell_4}|\cos\beta|\xi = \frac{\delta_3}{\ell_3}|\cos\alpha|\zeta\,, \tag{S55}$$

$$\frac{\delta_1}{\ell_1} = \frac{\delta_4}{\ell_4}\,, \tag{S56}$$

$$\frac{\delta_3}{\ell_3} = \frac{\delta_2}{\ell_2}\,. \tag{S57}$$

It can be easily verified that the above rotations are a compatible set with a single degree of freedom associated with bending of the panels i.e. choosing any one rotation independently will define a unique bending configuration of the unit cell. Additionally, it can be also be verified that these rotations satisfy the tessellation boundary conditions, i.e. $\angle O_1' O_2 O_3' = \angle O_7' O_8 O_9'$ and $\angle O_1' O_4 O_7' = \angle O_3' O_6 O_9'$.

C. Bending curvatures

We define the curvatures along each of the orthogonal directions $\mathbf{L} = \overrightarrow{O_1O_3}$ and $\mathbf{W} = \overrightarrow{O_1O_7}$ as the relative tilt of the triangular faces across the unit cell length in the respective directions. The curvature along $\mathbf{L}$ direction is given by,

$$\kappa_L = \frac{\text{sgn}\left[(\mathbf{n}\times\mathbf{L})\cdot(\mathbf{N}'_{369}\times\mathbf{N}_{369})\right]|\theta_{369}| - \text{sgn}\left[(\mathbf{n}\times\mathbf{L})\cdot(\mathbf{N}'_{147}\times\mathbf{N}_{147})\right]|\theta_{147}|}{L}\,. \tag{S58}$$

The curvature along $\mathbf{W}$ direction is given by,

$$\kappa_W = \frac{\text{sgn}\left[(\mathbf{n}\times\mathbf{W})\cdot(\mathbf{N}'_{789}\times\mathbf{N}_{789})\right]|\theta_{789}| - \text{sgn}\left[(\mathbf{n}\times\mathbf{W})\cdot(\mathbf{N}'_{123}\times\mathbf{N}_{123})\right]|\theta_{123}|}{W}\,, \tag{S59}$$

where, $\mathbf{n} = \mathbf{W}\times\mathbf{L}$, $|\theta_{123}|$, $|\theta_{789}|$, $|\theta_{147}|$, and $|\theta_{369}|$ are the respective angles between the normals $\mathbf{N}_{123}$, $\mathbf{N}_{789}$, $\mathbf{N}_{147}$, and $\mathbf{N}_{369}$ and $\mathbf{N}'_{123}$, $\mathbf{N}'_{789}$, $\mathbf{N}'_{147}$, and $\mathbf{N}'_{369}$. The angle between the face normals before and after bending represents the slope (or angle change) of each of the curves formed by the unit cells along the tessellation directions.

The angle change between the above normals can be calculated through their vector cross

product. We have,

$$
\begin{aligned}
(\mathbf{N}'_{123} \times \mathbf{N}_{123}) \frac{\cos^2\beta}{ca^4\cos^2\alpha} = &\left[\cos\alpha\zeta(\frac{\delta_2}{\ell_2}) + \cos\beta(\cos\alpha\cos\phi - \cos\beta)(\frac{\delta_1}{\ell_1})\right]\hat{\mathbf{i}} \\
&+ \left[\sin\alpha\zeta(\frac{\delta_2}{\ell_2})\right. \\
&\left. + \frac{(\cos\phi - \cos\alpha\cos\beta)(\cos\alpha\cos\phi - \cos\beta)}{\sin\alpha}(\frac{\delta_1}{\ell_1})\right]\hat{\mathbf{j}} \\
&+ \left[\sin\gamma_2\sin\beta(\cos\alpha\cos\phi - \cos\beta)(\frac{\delta_1}{\ell_1})\right]\hat{\mathbf{k}}\,.
\end{aligned}
$$

This gives us,

$$
|\mathbf{N}'_{123} \times \mathbf{N}_{123}|^2 \left[\frac{\cos^2\beta}{ca^4\cos^2\alpha}\right]^2 = (\frac{\delta_2}{\ell_2})^2\zeta^2 + (\frac{\delta_1}{\ell_1})^2\xi^2 - 2(\frac{\delta_2}{\ell_2})(\frac{\delta_1}{\ell_1})\zeta\xi\cos\phi\,.
$$

Using the constraint on bending rotations that relates δ_2 and δ_1 (Eqn. S54), the above expression can be simplified as,

$$
\begin{aligned}
|\mathbf{N}'_{123} \times \mathbf{N}_{123}|^2 \left[\frac{\cos^2\beta}{ca^4\cos^2\alpha}\right]^2 &= (\frac{\delta_1}{\ell_1})^2\xi^2\left[\frac{\cos^2\beta}{\cos^2\alpha} + 1 - 2\frac{\cos\beta}{\cos\alpha}\cos\phi\right] \\
&= (\frac{\delta_1}{\ell_1})^2\xi^2\frac{L^2}{b^2} \quad \text{(Using Eqns. S6, S8)}\,.
\end{aligned}
$$

This gives us,

$$
|\mathbf{N}'_{123} \times \mathbf{N}_{123}| = a^2b^2c\frac{|\delta_1|}{\ell_1}|\xi|\frac{L}{b}\,.
$$

Finally, noting that $|\mathbf{N}_{123}| = ab\sin\phi$, the angle change for the triangular face $(O_1O_2O_3)$ is given by

$$
|\theta_{123}| \approx \frac{|\mathbf{N}_{123} \times \mathbf{N}'_{123}|}{|\mathbf{N}_{123}|^2} = \frac{cL|\xi|}{b\sin^2\phi}\frac{|\delta_1|}{\ell_1}\,.
$$

In order to obtain the angle changes for each of the other triangular faces after bending, we conveniently choose a coordinate system that is oriented such that the x-axis is along the fold line that is connected to the triangular face and passing through O_5 and the xy-plane to coincide with one of the panels connected to the triangular face. This will allow us to

perform a similar calculation as above and produce the following result:

$$\left[\frac{|\mathbf{N}'_{789}\times\mathbf{N}_{789}|}{a^2b^2c}\right]^2 = (\frac{\delta_3}{\ell_3})^2\zeta^2 + (\frac{\delta_4}{\ell_4})^2\xi^2 - 2(\frac{\delta_3}{\ell_3})(\frac{\delta_4}{\ell_4})\zeta\xi\cos\phi\,,$$

$$\left[\frac{|\mathbf{N}'_{147}\times\mathbf{N}_{147}|}{c^4a}\right]^2 = (\frac{\delta_1}{\ell_1})^2\cos^2\alpha(1-\cos\psi)^2 + (\frac{\delta_4}{\ell_4})^2\cos^2\alpha(1-\cos\psi)^2 - 2(\frac{\delta_1}{\ell_1})(\frac{\delta_4}{\ell_4})\cos^2\alpha(1-\cos\psi)^2\cos\psi\,,$$

$$\left[\frac{|\mathbf{N}'_{369}\times\mathbf{N}_{369}|}{c^4b}\right]^2 = (\frac{\delta_3}{\ell_3})^2\cos^2\beta(1-\cos\psi)^2 + (\frac{\delta_2}{\ell_2})^2\cos^2\beta(1-\cos\psi)^2 - 2(\frac{\delta_3}{\ell_3})(\frac{\delta_2}{\ell_2})\cos^2\beta(1-\cos\psi)^2\cos\psi\,.$$

Simplying the above expressions using constraint Eqns. S54, S55, S56, S57 and noting that $|\mathbf{N}_{789}| = ab\sin\phi$, $|\mathbf{N}_{147}| = c^2\sin\psi$, $|\mathbf{N}_{369}| = c^2\sin\psi$, we can derive the following expressions for the angle changes

$$|\theta_{123}| \approx \frac{|\mathbf{N}_{123}\times\mathbf{N}'_{123}|}{|\mathbf{N}_{123}|^2} = \frac{cL\xi}{b\sin^2\phi}\frac{|\delta_1|}{\ell_1}\,, \tag{S60}$$

$$|\theta_{789}| \approx \frac{|\mathbf{N}_{789}\times\mathbf{N}'_{789}|}{|\mathbf{N}_{789}|^2} = \frac{cL\xi}{b\sin^2\phi}\frac{|\delta_1|}{\ell_1}\,, \tag{S61}$$

$$|\theta_{147}| \approx \frac{|\mathbf{N}_{147}\times\mathbf{N}'_{147}|}{|\mathbf{N}_{147}|^2} = \frac{aW\cos\alpha(1-\cos\psi)}{c\sin^2\psi}\frac{|\delta_1|}{\ell_1}\,, \tag{S62}$$

$$|\theta_{369}| \approx \frac{|\mathbf{N}_{369}\times\mathbf{N}'_{369}|}{|\mathbf{N}_{369}|^2} = \frac{aW\cos\beta(1-\cos\psi)}{c\sin^2\psi}\frac{\xi}{|\zeta|}\frac{|\delta_1|}{\ell_1}\,. \tag{S63}$$

The above expressions indicate that $|\theta_{123}| = |\theta_{789}|$ which is consistent with the presence of the plane of symmetry $(O_4O_5O_6)$. The symmetry also makes the expression for κ_W to be independent of whether the system is in eggbox or Miura mode. However, that is not the case for the curvature κ_L. The normals $\mathbf{N}'_{147}$, $\mathbf{N}'_{369}$ depend only on rotations δ_1, δ_4 and δ_2, δ_3 respectively. From Eqn. S55 (or S54), δ_4 (or δ_1) and δ_3 (or δ_2) have the same sign for eggbox mode and opposite sign for Miura mode. This is because, as noted before, from Eqn. S15, $\xi \geq 0$ (since $\gamma_1 \leq \pi$) throughout the configurational space and from Eqn. S16 $\zeta < 0$ when $\gamma_3 > \pi$. This makes the angle changes for faces $(O_1O_4O_7)$ and $(O_3O_6O_9)$ to have opposite sign for eggbox mode and same sign for Miura mode.

To calculate the curvatures, we consider the two cases depending on whether $\gamma_3 < \pi$ (eggbox mode) or $\gamma_3 > \pi$ (Miura mode), as outlined below.

Case-1: $\gamma_3 < \pi \implies \zeta > 0$ (eggbox mode)

$$\kappa_L = -\frac{|\theta_{369}| + |\theta_{147}|}{L}\,\mathrm{sgn}\,(\delta_1) = -\frac{aW(1-\cos\psi)}{cL\sin^2\psi}\,\frac{(\cos^2\alpha + \cos^2\beta - 2\cos\alpha\cos\beta\cos\phi)}{\zeta}\,\frac{|\delta_1|}{\ell_1}\,\mathrm{sgn}\,(\delta_1)\,, \tag{S64}$$

$$\kappa_W = -\frac{|\theta_{789}| + |\theta_{123}|}{W}\,\mathrm{sgn}\,(\delta_1) = -\frac{2cL\xi}{bW\sin^2\phi}\,\frac{|\delta_1|}{\ell_1}\,\mathrm{sgn}\,(\delta_1)\,. \tag{S65}$$

Case-2: $\gamma_3 > \pi \implies \zeta < 0$ (Miura mode)

$$\kappa_L = \frac{|\theta_{369}| - |\theta_{147}|}{L}\,\mathrm{sgn}\,(\delta_1) = -\frac{aW(1-\cos\psi)}{cL\sin^2\psi}\,\frac{(\cos^2\alpha + \cos^2\beta - 2\cos\alpha\cos\beta\cos\phi)}{\zeta}\,\frac{|\delta_1|}{\ell_1}\,\mathrm{sgn}\,(\delta_1)\,, \tag{S66}$$

$$\kappa_W = -\frac{|\theta_{789}| + |\theta_{123}|}{W}\,\mathrm{sgn}\,(\delta_1) = -\frac{2cL\xi}{bW\sin^2\phi}\,\frac{|\delta_1|}{\ell_1}\,\mathrm{sgn}\,(\delta_1)\,. \tag{S67}$$

We note that the curvatures κ_L in both the cases are of opposite sign due to the change in sign of ζ. However, the analytical expressions for the curvatures in both the cases are the same irrespective of the configuration change from eggbox to Miura mode.

D. Poisson's ratio in bending for the Morph pattern

The Poisson's ratio in bending ν^b_{WL} is defined as the ratio of curvatures in **W** and **L** directions [1, 2]. Using Eqns. S6 and S18 to simplify the above expressions of the curvatures, we can calculate the bending Poisson's ratio as,

$$\begin{aligned}
\nu^b_{WL} &= -\kappa_W/\kappa_L && \text{(S68)}\\
&= -\frac{2cL\xi}{aW(1-\cos\psi)}\,\frac{\zeta}{(\cos^2\alpha + \cos^2\beta - 2\cos\alpha\cos\beta\cos\phi)}\,\frac{cL\sin^2\psi}{bW\sin^2\phi}\\
&= -\frac{2c^2L^2\xi}{a^2W^2(1-\cos\psi)}\,\frac{\zeta}{(\cos^2\frac{\psi}{2}\sin^2\phi)}\left|\frac{\cos\beta}{\cos\alpha}\right|\frac{\sin^2\psi}{\sin^2\phi}\\
&= -\frac{4c^2L^2}{a^2W^2}\left|\frac{\cos\beta}{\cos\alpha}\right|\frac{\xi\zeta}{\sin^4\phi}\,. && \text{(S69)}
\end{aligned}$$

By comparing with Eqn. S20, for the Morph pattern, we reach the elegant result,

$$\nu^s_{WL} = -\nu^b_{WL}\,, \tag{S70}$$

i.e., the Poisson's ratios in stretching and bending are equal in magnitude and opposite in sign (see Fig. S8(a)), which is a remarkable property. This geometric property holds in

both the eggbox mode and the Miura mode and is independent of the material properties and length scale of the system. In sections V and VI, we show that our results generalize the previous results of the literature. In particular, we show that the expressions for the Poisson's ratio in stretch and bending for the standard eggbox and standard Miura-ori can be obtained as particular cases of our general derivation.

E. Out-of-plane bending stiffness for the Morph pattern

The bending energy per unit cell is given by,

$$\mathcal{U}_b = \frac{1}{2} W L B_W \kappa_W^2 = \frac{1}{2} W L B_L \kappa_L^2 \,, \tag{S71}$$

where, B_W and B_L are the bending stiffness of the tessellation per unit width in **W** and **L** directions respectively. But, as discussed before, the bending is assumed to be solely due to the bending of the four panels. Hence, we can also write,

$$\mathcal{U}_b = \ell_1 \mathcal{F}(\delta_1) + \ell_2 \mathcal{F}(\delta_2) + \ell_3 \mathcal{F}(\delta_3) + \ell_4 \mathcal{F}(\delta_4) \,, \tag{S72}$$

where, $\mathcal{F}(\delta_i) = \frac{1}{2} k_b \delta_i^2$ is the energy per unit length along the bending lines which are modeled as bending rotational hinges across panel diagonals and k_b is the stiffness constant associated with those hinges. Since, $\ell_1 = \ell_4$, $\ell_3 = \ell_2$ for Morph, we have, $\delta_1 = \delta_4$, $\delta_3 = \delta_2$ using Eqns. S56, S57. So,

$$\mathcal{U}_b = k_b (\ell_1 \delta_1^2 + \ell_3 \delta_3^2) \,. \tag{S73}$$

Now, using Eqn. S54, we have,

$$\mathcal{U}_b = k_b \frac{\delta_1^2}{\ell_1^2} \left[\frac{\ell_1^3 \cos^2 \alpha \zeta^2 + \ell_3^3 \cos^2 \beta \xi^2}{\cos^2 \alpha \zeta^2} \right] . \tag{S74}$$

Comparing Eqns. S71 and S74 and using the expressions for curvatures from previous subsection, we get the analytical expressions for the bending stiffnesses as given below,

$$B_W = \frac{k_b b^2 W \sin^4 \phi}{2 c^2 L^3 \cos^2 \alpha} \left[\frac{\ell_1^3 \cos^2 \alpha \zeta^2 + \ell_3^3 \cos^2 \beta \xi^2}{\xi^2 \zeta^2} \right] , \tag{S75}$$

$$B_L = \frac{2 k_b a^2 c^2 (1 + \cos \psi)^2}{W^3 L^3 \cos^2 \beta} \left[\frac{\ell_1^3 \cos^2 \alpha \zeta^2 + \ell_3^3 \cos^2 \beta \xi^2}{\cos^2 \alpha \cos^2 \beta} \right] . \tag{S76}$$

The bending stiffnesses are related to bending Poisson's ratio as $(\nu_{WL}^b)^2 = B_L / B_W$. This can be easily observed by comparing Eqns. S71 and S68. The above analytical expressions

are plotted in Fig. S8(b). For numerical simulation of bending, we consider a pattern with 21×21 cells and calculate curvatures from unit cells at the center of the system. The moments are applied in a way similar to reference [1].

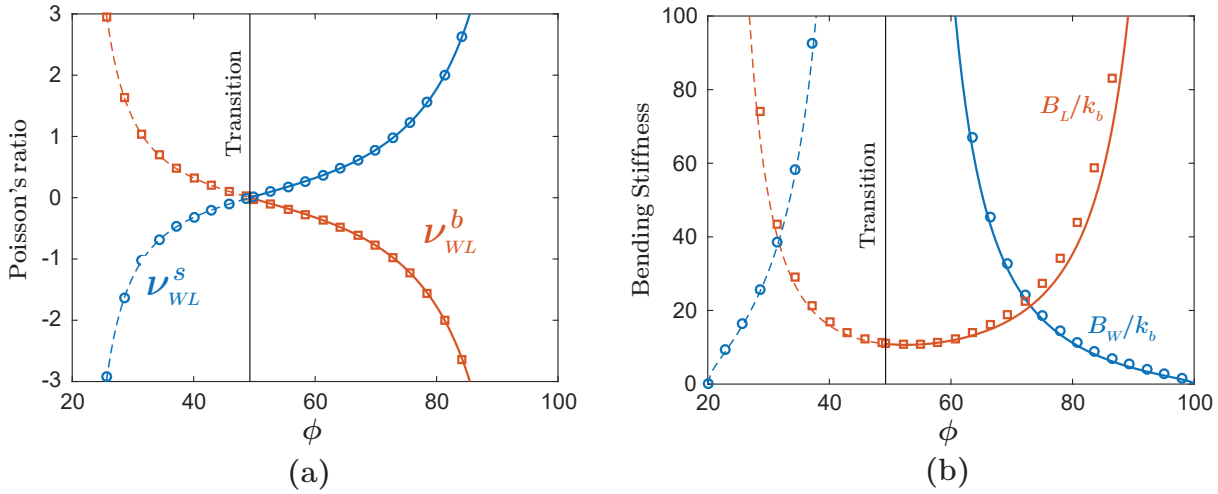

FIG. S8. (a) Comparison of Poisson's ratio in bending and stretching. (b) Normalized out-of-plane bending stiffness of Morph unit cell. B_W and B_L represent the bending stiffnesses per unit width along **W** and **L** directions respectively. In both the figures, $\alpha = 60°$ and $\beta = 40°$. The dashed lines represent the results in the Miura mode and the solid lines represent the results in the eggbox mode. The circle and square markers show the numerical results obtained using the bar and hinge model.

V. RECOVERY OF STANDARD EGGBOX RELATIONSHIPS FROM MORPH

In this section, we show that, all the results derived for Morph can be reduced to the special case of standard eggbox that has been well studied in the literature, by setting $\beta = \alpha$ and $a = b$. From Eqn. S18, the relation between ϕ and ψ becomes:

$$\begin{aligned} \cos^2\frac{\psi}{2} &= \frac{\cos^2\alpha + \cos^2\beta - 2\cos\alpha\cos\beta\cos\phi}{\sin^2\phi} \\ &= 2\cos^2\alpha\frac{(1-\cos\phi)}{1-\cos^2\phi} \\ &= \frac{\cos^2\alpha}{\cos^2\frac{\phi}{2}}, \\ \implies \cos\frac{\phi}{2}\cos\frac{\psi}{2} &= \cos\alpha\,. \end{aligned} \tag{S77}$$

Since, for standard eggbox, $L = 2a\sin\frac{\phi}{2}$ and $W = 2c\sin\frac{\psi}{2}$, we have,

$$\begin{aligned}
\nu^s_{WL} &= \frac{4c^2L^2}{a^2W^2}\left|\frac{\cos\beta}{\cos\alpha}\right|\frac{\xi\zeta}{\sin^4\phi} \\
&= \frac{\sin^2\frac{\phi}{2}}{\sin^2\frac{\psi}{2}}\frac{4\cos^2\alpha(1-\cos\phi)^2}{(1-\cos^2\phi)^2} \\
&= \frac{\sin^2\frac{\phi}{2}}{\sin^2\frac{\psi}{2}}\frac{\cos^2\frac{\phi}{2}\cos^2\frac{\psi}{2}}{\cos^4\frac{\phi}{2}} = \frac{\tan^2\frac{\phi}{2}}{\tan^2\frac{\psi}{2}}\,, \\
\implies \nu^s_{WL} &= \frac{\tan^2\frac{\phi}{2}}{\tan^2\frac{\psi}{2}}\,.
\end{aligned} \tag{S78}$$

which is in agreement with the expression previously derived by [2, 3].

Next, we obtain the expressions for bending curvatures from Eqns. S64, S65.

$$\begin{aligned}
\kappa_L &= -\frac{aW(1-\cos\psi)}{cL\sin^2\psi}\frac{(\cos^2\alpha+\cos^2\beta-2\cos\alpha\cos\beta\cos\phi)}{\zeta}\frac{|\delta_1|}{\ell_1}\operatorname{sgn}(\delta_1) \\
&= -\frac{\sin\frac{\psi}{2}}{\sin\frac{\phi}{2}}\frac{2\cos\alpha(1-\cos\phi)}{(1+\cos\psi)(1-\cos\phi)}\frac{|\delta_1|}{\ell_1}\operatorname{sgn}(\delta_1) \\
&= -\frac{\tan\frac{\psi}{2}}{\tan\frac{\phi}{2}}\frac{|\delta_1|}{\ell_1}\operatorname{sgn}(\delta_1)\,,
\end{aligned} \tag{S79}$$

$$\begin{aligned}
\kappa_W &= -\frac{2cL\xi}{bW\sin^2\phi}\frac{|\delta_1|}{\ell_1}\operatorname{sgn}(\delta_1) \\
&= -\frac{2\sin\frac{\phi}{2}}{\sin\frac{\psi}{2}}\frac{2\cos\alpha}{(1+\cos\phi)}\frac{|\delta_1|}{\ell_1}\operatorname{sgn}(\delta_1) \\
&= -\frac{\tan\frac{\phi}{2}}{\tan\frac{\psi}{2}}\frac{|\delta_1|}{\ell_1}\operatorname{sgn}(\delta_1)\,.
\end{aligned} \tag{S80}$$

The bending Poisson's ratio is now obtained as,

$$\nu^b_{WL} = -\kappa_W/\kappa_L = -\frac{\tan^2\frac{\phi}{2}}{\tan^2\frac{\psi}{2}}\,. \tag{S81}$$

These results are in agreement with Eqns. S48, S49 and S50 that we derived previously for bending of the standard eggbox, and with reference [3].

VI. RECOVERY OF STANDARD MIURA-ORI RELATIONSHIPS FROM MORPH

In this section, we show that, all the results derived for Morph can be reduced to the special case of standard Miura-ori that has been well studied in the literature, by setting

$\beta = \pi - \alpha$ and $a = b$. From Eqn. S18, the relation between ϕ and ψ becomes:

$$\begin{aligned}
\cos^2\frac{\psi}{2} &= \frac{\cos^2\alpha + \cos^2\beta - 2\cos\alpha\cos\beta\cos\phi}{\sin^2\phi} \\
&= 2\cos^2\alpha\frac{(1+\cos\phi)}{1-\cos^2\phi} \\
&= \frac{\cos^2\alpha}{\sin^2\frac{\phi}{2}}\,, \\
\implies \sin\frac{\phi}{2}\cos\frac{\psi}{2} &= |\cos\alpha|\,.
\end{aligned} \tag{S82}$$

Since, for standard Miura-ori, $L = 2a\sin\frac{\phi}{2}$ and $W = 2c\sin\frac{\psi}{2}$, we have,

$$\begin{aligned}
\nu^s_{WL} &= \frac{4c^2L^2}{a^2W^2}\left|\frac{\cos\beta}{\cos\alpha}\right|\frac{\xi\zeta}{\sin^4\phi} \\
&= -\frac{\sin^2\frac{\phi}{2}}{\sin^2\frac{\psi}{2}}\frac{4\cos^2\alpha(1+\cos\phi)^2}{(1-\cos^2\phi)^2} \\
&= -\frac{\sin^2\frac{\phi}{2}}{\sin^2\frac{\psi}{2}}\frac{\sin^2\frac{\phi}{2}\cos^2\frac{\psi}{2}}{\sin^4\frac{\phi}{2}} = -\cot^2\frac{\psi}{2}\,, \\
\implies \nu^s_{WL} &= -\cot^2\frac{\psi}{2}\,.
\end{aligned} \tag{S83}$$

which is in agreement with the expression previously derived by [1, 2].

Next, we obtain the expressions for bending curvatures from Eqns. S64, S65.

$$\begin{aligned}
\kappa_L &= -\frac{aW(1-\cos\psi)}{cL\sin^2\psi}\frac{(\cos^2\alpha + \cos^2\beta - 2\cos\alpha\cos\beta\cos\phi)}{\zeta}\frac{|\delta_1|}{\ell_1}\operatorname{sgn}(\delta_1) \\
&= -\frac{\sin\frac{\psi}{2}}{\sin\frac{\phi}{2}}\frac{2\cos\alpha(1+\cos\phi)}{(1+\cos\psi)(1+\cos\phi)}\frac{|\delta_1|}{\ell_1}\operatorname{sgn}(\delta_1) \\
&= -\frac{\sin\frac{\psi}{2}}{\sin\frac{\phi}{2}}\frac{2\cos\alpha}{(1+\cos\psi)}\frac{|\delta_1|}{\ell_1}\operatorname{sgn}(\delta_1)\,,
\end{aligned} \tag{S84}$$

$$\begin{aligned}
\kappa_W &= -\frac{2cL\xi}{bW\sin^2\phi}\frac{|\delta_1|}{\ell_1}\operatorname{sgn}(\delta_1) \\
&= \frac{\sin\frac{\phi}{2}}{\sin\frac{\psi}{2}}\frac{2\cos\alpha}{(1-\cos\phi)}\frac{|\delta_1|}{\ell_1}\operatorname{sgn}(\delta_1)\,.
\end{aligned} \tag{S85}$$

The bending Poisson's ratio is now obtained as,

$$\nu^b_{WL} = -\kappa_W/\kappa_L = \cot^2\frac{\psi}{2}\,. \tag{S86}$$

These results are in agreement with that obtained by [1] for bending of standard Miura-ori.

VII. HYBRID PATTERNS

The configuration space of a Morph pattern is described in terms of the angles ϕ and ψ. Similarly, we use the angles ϕ_e, ψ_e and ϕ_m, ψ_m (see Fig. S11) to describe the configuration space of the hybrid patterns in terms of the unit cells in eggbox and Miura modes respectively. In this section, we derive the relation between these angles and also derive an analytical expression for the global in-plane Poisson's ratio of a general hybrid pattern. We then discuss the phenomenon of mode locking in hybrid patterns.

A. Configuration space of hybrid patterns

The rigid foldability between various hybrid patterns is only possible when all unit cells are first brought to the transition state (see Fig. S9). From Fig. S10, we can see that a horizontal line intersects the configuration path at two points say $(\phi_e, \psi_e = \psi)$ and $(\phi_m, \psi_m = \psi)$. Any unit cell of a given hybrid pattern should conform to one or the other of these two points depending on whether the unit is in eggbox or Miura mode. From this hybrid state if ψ of all the unit cells is increased by folding simultaneously (such that $\psi_e = \psi_m = \psi$ still holds), then, based on Fig. S10, ϕ_e starts decreasing and ϕ_m starts increasing until $\phi_e = \phi_m = \phi_T$, where, ϕ_T $(\phi_m \leq \phi_T \leq \phi_e)$ is the angle ϕ when the unit cells reach the transition point. This shows that it is kinematically possible to take any hybrid pattern into a state where all unit cells are in transition mode. From the transition state, by following a reverse process but with different rows of unit cells triggered to go into Miura/eggbox modes, various other hybrid configurations can be obtained from the same pattern.

Below, we quantify the geometries during the hybrid transformations. From Fig. S11, we can see that $\phi_e = \phi_1 + \phi_2$ and $\phi_m = \phi_1 - \phi_2$. In order to place the eggbox and Miura mode unit cells adjacent to each other, they should meet the compatibility condition that $\psi_e = \psi_m = \psi$. From the orthogonality of the unit cell (see Eqns. S1 and S4) we have,

$$\frac{b}{a} = \frac{\cos\alpha}{\cos\beta} = \frac{\cos\phi_1}{\cos\phi_2} \tag{S87}$$

where, $\phi_1 \to \alpha$ and $\phi_2 \to \beta$ in the limit of approaching the flat-folded states. Also, from Eqns. S8 and S18, we have,

$$\cos\frac{\psi}{2} = \frac{L\cos\alpha}{b\sin\phi} = \frac{L\cos\beta}{a\sin\phi} \tag{S88}$$

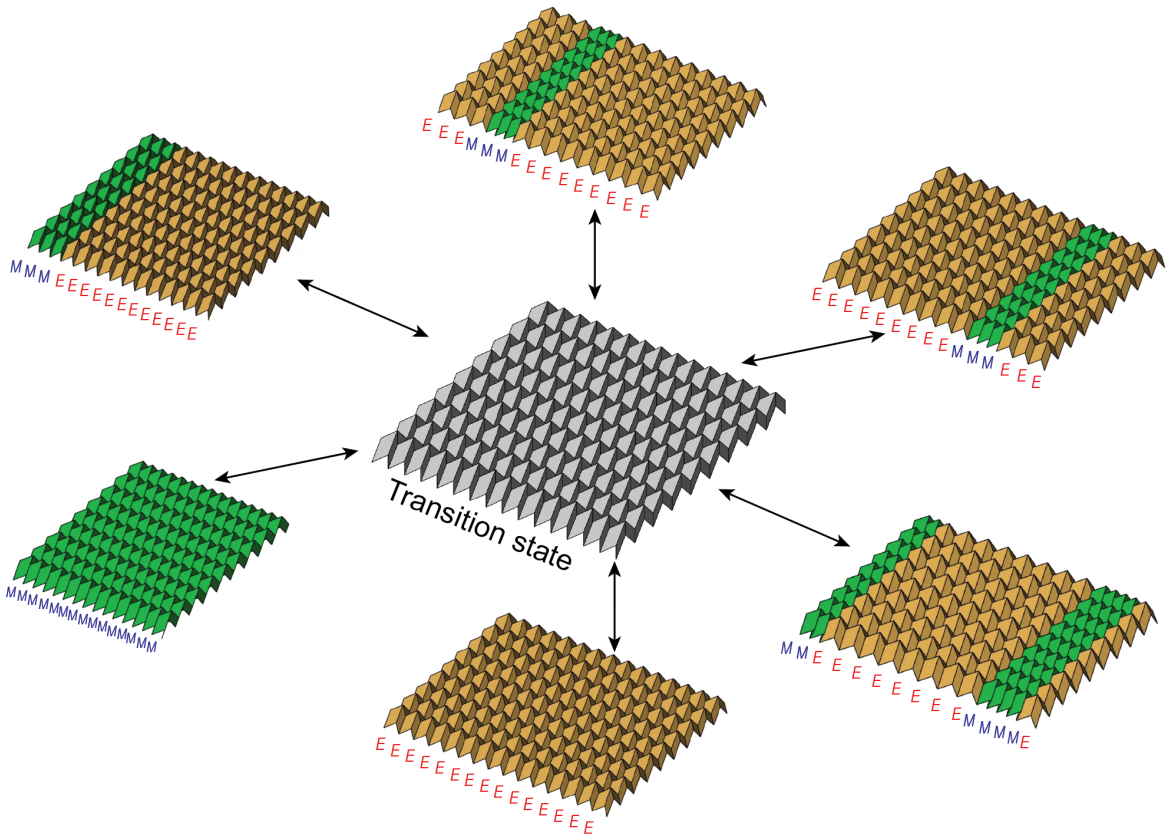

FIG. S9. The Morph pattern transforms into various hybrid patterns via the transition state. The hybrid pattern is a composite metamaterial system that can morph into any combination of Miura (denoted by M, shown in green color) and eggbox (denoted by E, shown in yellow color) modes, which have contrasting mechanical properties. This leads to a reprogrammable and in-situ tunable metamaterial.

Noting that, $L = a\sin\phi_1 \pm b\sin\phi_2$, we can also show that, $\sin\phi = \sin(\phi_1 \pm \phi_2) = L\cos\phi_1/b = L\cos\phi_2/a$. Using these relations, we can calculate ϕ_1 and ϕ_2 for a given ψ as,

$$\cos\phi_1 = \frac{\cos\alpha}{\cos\frac{\psi}{2}} \tag{S89}$$

$$\cos\phi_2 = \frac{\cos\beta}{\cos\frac{\psi}{2}} \tag{S90}$$

from which $\phi_e = \phi_1 + \phi_2$ and $\phi_m = \phi_1 - \phi_2$ can be calculated as,

$$\phi_e = \cos^{-1}\left(\frac{\cos\alpha}{\cos\frac{\psi}{2}}\right) + \cos^{-1}\left(\frac{\cos\beta}{\cos\frac{\psi}{2}}\right) \tag{S91}$$

$$\phi_m = \cos^{-1}\left(\frac{\cos\alpha}{\cos\frac{\psi}{2}}\right) - \cos^{-1}\left(\frac{\cos\beta}{\cos\frac{\psi}{2}}\right) \tag{S92}$$

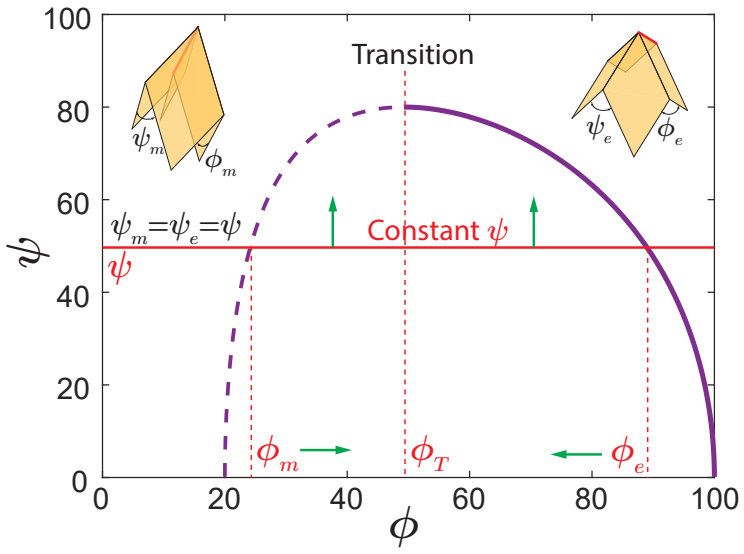

FIG. S10. Configuration space of a Morph unit cell with $\alpha = 60°$ and $\beta = 40°$. As a line of constant ψ moves upwards towards transition point, ϕ_m and ϕ_e converge towards ϕ_T.

As the system folds into hybrid modes from the transition point, the above two equations dictate the angles ϕ_e and ϕ_m of the eggbox and Miura mode unit cells respectively, for a given ψ that is equal across all the unit cells.

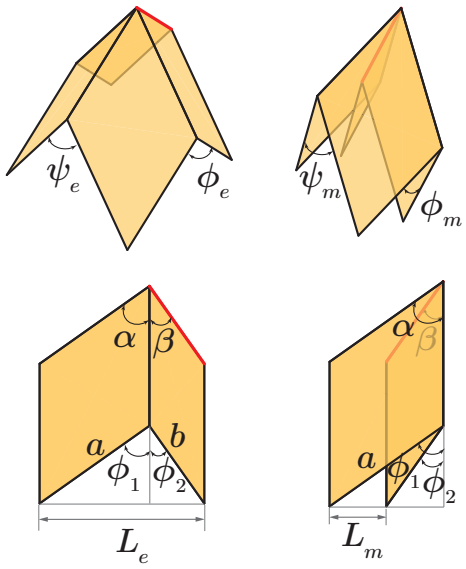

FIG. S11. Unit cells of hybrid patterns in the eggbox and Miura modes. For compatibility, $\psi_e = \psi_m = \psi$ with $\phi_e = \phi_1 + \phi_2$ and $\phi_m = \phi_1 - \phi_2$.

B. Stretch Poisson's ratio of hybrid patterns

We define the length and width of the pattern of $n \times n$ unit cells as, $L' = n_e L_e + n_m L_m$ and $W' = nW$ respectively, where, $n = n_e + n_m$ with n_e denoting number of eggbox mode strips and n_m denoting the number of Miura mode strips (see Fig. S12). The unit cell lengths in the two modes are given by,

$$L_e^2 = a^2 + b^2 - 2ab\cos\phi_e\,, \tag{S93}$$

$$L_m^2 = a^2 + b^2 - 2ab\cos\phi_m\,. \tag{S94}$$

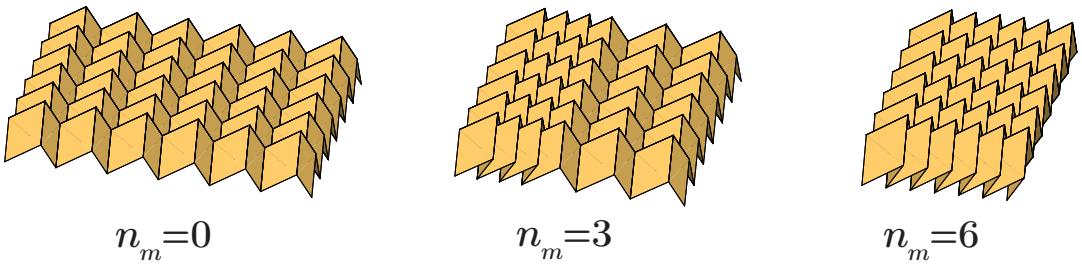

FIG. S12. Hybrid patterns with varying number of Miura strips, n_m, for $n = 6$.

The Poisson's ratio in stretch of the hybrid pattern is then defined as,

$$\nu^s_{WL,h} = -\frac{\mathrm{d}L'/L'}{\mathrm{d}W'/W'} = -\frac{W'}{L'}\frac{\mathrm{d}L'}{\mathrm{d}\psi}\frac{\mathrm{d}\psi}{\mathrm{d}W'}\,. \tag{S95}$$

In the above notation for the Poisson's ratio, the "h" in the subscript indicates the "hybrid" pattern. The derivatives are obtained as,

$$\frac{\mathrm{d}L'}{\mathrm{d}\psi} = n_e\frac{\mathrm{d}L_e}{\mathrm{d}\psi} + n_m\frac{\mathrm{d}L_m}{\mathrm{d}\psi}\,, \tag{S96}$$

$$\frac{\mathrm{d}W'}{\mathrm{d}\psi} = n\frac{\mathrm{d}W}{\mathrm{d}\psi} = nc\cos\frac{\psi}{2}\,. \tag{S97}$$

Using Eqns. S89 and S90 and noting that $\phi_e = \phi_1 + \phi_2$, $\phi_m = \phi_1 - \phi_2$, we can derive the following analytical expression for in-plane Poisson's ratio of hybrid patterns:

$$\nu^s_{WL,h} = \frac{ab\sin^2\frac{\psi}{2}}{L'\cos^3\frac{\psi}{2}}\left[\frac{\cos\alpha}{\sin\phi_1}\left(\frac{n_e\sin\phi_e}{L_e} + \frac{n_m\sin\phi_m}{L_m}\right) + \frac{\cos\beta}{\sin\phi_2}\left(\frac{n_e\sin\phi_e}{L_e} - \frac{n_m\sin\phi_m}{L_m}\right)\right]. \tag{S98}$$

It is easy to show that when $\nu^s_{WL,h} = 0$, the ratio n_m/n_e depends only on the folded state of the system given by ψ and α, β. Therefore, it is possible to tune the switching of Poisson's ratio to occur at different folded states by appropriately choosing the ratio n_m/n_e.

C. Mode locking during in-plane deformation

A Morph pattern can be transformed into various hybrid patterns through smooth kinematics of the system. In practice, this could be achieved by applying in-plane rigid origami deformations (stretching) to the hybrid system. The ability of a hybrid pattern to transform into a different hybrid pattern depends on whether the applied deformations allow the individual unit cells to move away from or towards the transition point. When the global stretching (either extension or contraction) of the system causes the unit cells to move away from the transition (i.e. both ψ_e and ψ_m decrease), the unit cells are locked to remain in the existing eggbox and Miura modes without any further scope for mode morphing (see Figs. S13(a),(b)). On the other hand, when the global stretching of the system causes the unit cells to move towards the transition (i.e. both ψ_e and ψ_m increase), it is possible for the eggbox and the Miura modes to interchange (see Figs. S13(c),(d)). As shown in Fig. S13, it is possible to obtain either mode locking or mode morphing by appropriately applying extension or contraction on hybrid patterns that have positive or negative global Poisson's ratio.

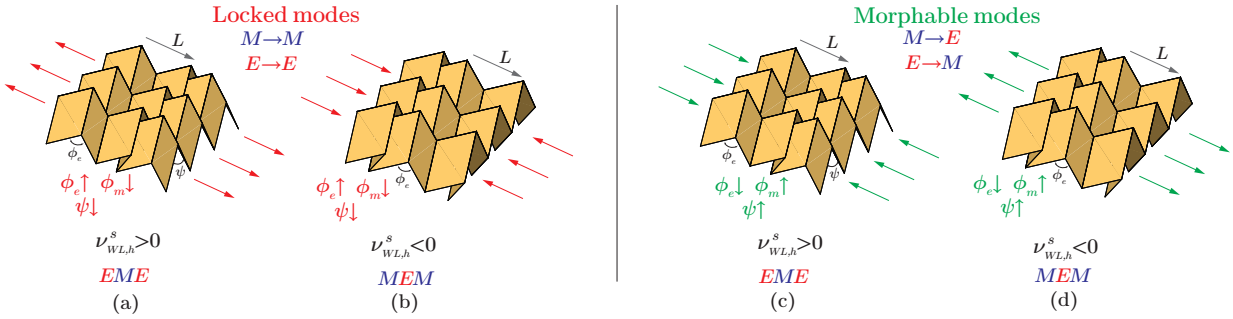

FIG. S13. In-plane stretching of hybrid patterns. (a), (b) Mode locking phenomenon in which the Miura (M) and eggbox (E) mode cells cannot change their mode as the deformation takes them away from transition. (c), (d) Deformations that take the Miura and eggbox mode unit cells towards transition enabling morphability of hybrid patterns.

VIII. VIDEO CAPTIONS

Video 1 *Origami modes and locking*

A paper based Morph origami model is used to demonstrate the modes in its configurational space and the corresponding flat-folded states. Further, it is transformed into a hybrid pattern (with one strip of cells in Miura mode and all others in eggbox mode) to demonstrate tensile mode locking.

Video 2 *Morphing of Morph pattern*

Traversal of the configuration space of a Morph pattern where it can smoothly transition between eggbox, Miura and Hybrid modes as a rigid origami is demonstrated through simulation.

Video 3 *Hybrid origami patterns*

A large paper based model of Morph pattern with 10×10 cells is used to demonstrate deformation shapes under bending in eggbox and Miura modes as well as for the hybrid patterns.

Video 4 *Rigid morphing into hybrid*

A paper/plastic based Morph model with three unit cells connected along the **L** direction is used to demonstrate the transformation from an all eggbox mode to a hybrid mode through rigid kinematics i.e. without any panel deformation. The Morph model is fabricated using extremely compliant hinges and relatively very stiff panels in order to approximate rigid origami behavior .

NOMENCLATURE

α, β	panel angles
γ_i, $i = 1$ to 4	dihedral angles between panels
ϕ, ψ	angles between opposite crease lines
a, b, c	edge lengths of panels
O_i, $i = 1$ to 9	vertices of a unit cell
L, W	length and width of a unit cell
L, **W**	vectors denoting $\overrightarrow{O_1O_3}$ (length) and $\overrightarrow{O_1O_7}$ (width)
ν^s_{WL}	Poisson's ratio in stretching

$\mathcal{E}$	energy stored per unit length in the folding rotational hinges
k_f	stiffness constant per unit length of folding rotational hinges
$\gamma_{i,0}$, $i = 1$ to 4	dihedral angles between panels in the undeformed configuration
$\mathcal{U}_s$	total energy in the unit cell due to in-plane stretching
K_W, K_L	stretching stiffnesses of the unit cell along **W**, **L** directions
δ_i, $i = 1, 2, 3, 4, 7, 8$	infinitesimal rotations about panel diagonals to model bending
O_i', $i = 1$ to 9	vertices of a unit cell after bending deformation
$\mathbf{N}_i$, $i = 123, 369, 147, 789$	normals of triangular faces before bending deformation
$\mathbf{N}_i'$, $i = 123, 369, 147, 789$	normals of triangular faces after bending deformation
ℓ_i, $i = 1$ to 4	lengths of shorter diagonals of the panels
θ_i, $i = 123, 369, 147, 789$	angle change between normals due to bending deformation
κ_L, κ_W	curvatures along **L**, **W** directions
ν_{WL}^b	Poisson's ratio in bending
$\mathcal{F}$	energy stored per unit length in the bending rotational hinges
$\mathcal{U}_b$	total energy in the unit cell due to out-of-plane bending
B_W, B_L	bending stiffnesses per unit width along **W**, **L** directions
k_b	stiffness constant per unit length of bending rotational hinges
ϕ_e, ψ_e	angles between opposite crease lines in eggbox mode
ϕ_m, ψ_m	angles between opposite crease lines in Miura mode
ϕ_1, ϕ_2	angles between panel edges and altitudes of triangles 123 or 789
L', W'	global length and width of a hybrid pattern
L_e	length of unit cell in eggbox mode
L_m	length of unit cell in Miura mode
n_e	number of eggbox mode strips in the hybrid pattern
n_m	number of Miura mode strips in the hybrid pattern
$\nu_{WL,h}^s$	global Poisson's ratio in stretching of the hybrid pattern

[1] Z. Y. Wei, Z. V. Guo, L. Dudte, H. Y. Liang, and L. Mahadevan, Physical Review Letters **110**, 215501 (2013).

[2] M. Schenk and S. D. Guest, Proceedings of the National Academy of Sciences **110**, 3276 (2013).

[3] H. Nassar, A. Lebée, and L. Monasse, Proceedings of the Royal Society - A **473**, 20160705 (2017).

[4] R. M. Murray, Z. Li, and S. S. Sastry, *A mathematical introduction to robotic manipulation* (CRC press, 1994).